Optimal Scheduling of Battery Charging Station Serving Electric Vehicles Based on Battery Swapping

Xiaoqi Tan, Guannan Qu, Bo Sun, Na Li, and Danny H.K. Tsang

***Abstract*—A battery charging station (BCS) is a charging facility that supplies electric energy for recharging electric vehicles' depleted batteries (DBs). A BCS has a certain number of charging bays and maintains a dynamic inventory of fully-charged batteries (FBs). This paper studies a BCS scheduling (BCSS) problem whose target is to schedule the charging processes of the charging bays such that the charging cost is minimized while satisfying the FB demand. Specifically, the BCSS problem has two types of operations: i) loading DBs into the charging bays and then unloading them to the FB inventory when they are fully-charged, and ii) controlling the charging rate of each charging bay. We formulate the BCSS problem as a mixed-integer program with quadratic battery degradation cost. A generalized Benders decomposition algorithm is then developed to solve the problem efficiently. The salience of the developed algorithm is that i) each charging bay can solve its own subproblem separately, and ii) each subproblem can be further partitioned into multiple simple quadratic programming problems, and thus the algorithm facilitates an efficient parallel implementation. We perform extensive real data simulation to validate the optimization model and demonstrate the efficiency of the proposed algorithm.**

***Index Terms*—Battery Charging Station, Charging Scheduling, Electric Vehicles, Generalized Benders Decomposition, Battery Swapping**

NOMENCLATURE

Acronyms

BCS	Battery Charging Station
BCSS	Battery Charging Station Scheduling
BDC	Battery Degradation Cost
BSS	Battery Swapping Station
CB	Charging Bay
DB	Depleted Battery
EPC	Electricity Purchasing Cost
FB	Fully-Charged Battery
SoC	State-of-Charge of batteries

Indices and Parameters

α	The minimum level of SoC for a battery to be regarded as fully-charged.
Δ_T	The length of each time slot.
η_b	Charging efficiency of the b-th CB.
$\mathcal{B}$	Set of all CBs.
$\mathcal{G}_b(\cdot)$	The battery degradaction cost function.
$\mathcal{T}$	Set of time slots $\{0, \cdots, T-1\}$.
CB_b	The b-th CB.
θ	The capacity of batteries.
B	Total number of charging bays.
b	Index for CBs.
C	Transmission line capacity
d_t	FB demand at time t
F_t	Total number of FBs at time t.
L_t	Non-battery load at time slot t
p_t	Electricity price at time slot t.
$r_b^{\max}$	Maximum charging rate of CB_b.
$s_{b,t}$	SoC of the battery in CB_b at time t.
$s_{b,t}^{\mathrm{new}}$	SoC of the newly-loaded battery in CB_b at t.
s_b^{initial}	Initial SoC of battery in CB_b.
T	Total number of time slots.

Decision Variables

$r_{b,t}$	Continuous decision variable: charging rate of the battery in CB_b at time slot t.
$u_{b,t}$	Binary decision variable: '1' if the battery in CB_b at time t is unloaded; '0' otherwise.

X. Tan, B. Sun, and D.H.K. Tsang are with the Department of Electronic and Computer Engineering, Hong Kong University of Science and Technology, Hong Kong (E-mail: {xtanaa, bsunaa, eetsang}@ust.hk). Guannan Qu and Na Li are with the School of Engineering and Applied Science, Harvard University (E-mail: gqu@g.harvard.edu, lina@seas.harvard.edu).

I. INTRODUCTION

As the adoption rate of electric vehicles (EVs) is increasing, there is a growing demand for fast and convenient energy refueling services. Currently, EV energy refueling is mainly performed by several well-known charging methods, such as slow charging at home [1] and fast charging at public charging stations [2]. However, many EVs, especially electric buses and taxis, have started to support swappable batteries [3], [4], and this facilitates an alternative EV energy refueling method, i.e., the battery-swapping method [5], [6].

Compared to the long charging time of existing charging methods (usually in hours), with the battery-swapping method an EV can swap its *depleted battery* (DB) for a *fully-charged battery* (FB) one at a battery swapping station (BSS) within several minutes [3], or even in tens of seconds [6]. The swapped DBs from different BSSs can be gathered together and recharged at a centralized battery charging station (BCS), which thus forms a gigantic battery energy storage system. It is believed that if appropriately planned and managed, the battery-swapping technology can not only benefit EV owners with a fast energy refueling service [7], but it can also provide enormous flexibility for grid operators to perform critical tasks such as load balancing [8] and renewable energy integration [9], [10], thus reducing carbon emissions [11] and improving the efficiency and stability of power systems [12].

A. Related Work

Undoubtedly, successful implementation of an EV energy refueling system based on battery swapping necessitates a well-designed scheduling strategy for BCSs. To this end, an increasing amount of research from the communities of power engineering (e.g., [13]–[17]) and operations research

(e.g., [18]–[20]) has started to investigate the modeling and scheduling of BCSs from different perspectives. For example, in [16], the authors studied the optimal cost-effective operation of a BCS with an uncertain electricity price and uncertain FB demand, and services such as battery-to-grid and battery-to-battery were discussed. Recently, the authors of [17] investigated the optimal charging scheduling of a BCS serving electric buses. Since the operation of electric buses is usually predictable, they assumed that each charging bay (CB) in the BCS had a fixed and known battery-swapping request. In [18], the optimal charging and discharging policies for maximizing the expected total profit over a fixed time horizon were proposed. Different from [18], the authors of [19] investigated the joint optimization of the battery charging and purchasing strategies for a single BCS and a network of BCSs. Therefore, the long-term investment in batteries and the short-term operational cost could be balanced. The work in this paper is also particularly related to [20], in which the authors defined the scheduling of a BCS as a new inventory management problem. The main task of this inventory management problem was the development of an optimal charging strategy that optimizes the corresponding objective and satisfies the FB demand simultaneously.

Despite the aforementioned work, the following three important aspects of a BCS have not been fully investigated by the existing work in a unified framework.

- **Charging rates are continuously-controllable**. As mentioned in our previous work [21], the fixed charging rate is easier to be implemented because it only requires a simple on/off switching control. However, it is also much less flexible for providing grid services. In comparison, the continuously-controllable charging rate is more flexible although it requires more sophisticated charging devices. For the sake of simplicity, the charging rates were assumed to be fixed in many existing work such as [19], [20]. However, with the advancement of battery technology, it is becoming more practical and important to have a scheduling method for BCS with continuously-controllable charging rates. We consider a general optimization framework for the scheduling of BCS must take this factor into account.
- **FBs should have minimum energy levels**. It might be acceptable to provide a half-charged battery for an EV under some special circumstances. However, in general, it is better to ensure that the state-of-charge (SoC) of a FB is close to fully-charged. To this end, both the authors of [16] and [20] introduced a weighted penalty term in the corresponding objective to penalize those unbalanced battery capacities. Unfortunately, there is no systematic way to tune the weighting parameters in the objective function to strike an optimal balance between the charging cost (usually in the unit of dollar) and the artificial penalty (usually has no unit). Moreover, even the optimal weighting parameter can be found, it is still difficult to ensure a good battery-swapping service among all EVs since the SoCs of FBs are not guaranteed to exceed a certain minimum energy level.
- **The number of CBs is limited and FBs should be warehoused**. For a BCS in practice [3], [22], the total number of CBs is usually limited and much smaller than the total number of batteries. Once a battery is fully-charged, this battery must be unloaded from the corresponding CB and then stored in a warehouse (i.e., the FB inventory). Meanwhile, a new battery will be loaded to this CB to continue the charging process. However, most existing work neglected such type of operation in reality. For instance, it was implicitly assumed in [16], [17], [20] that each battery is connected with a CB and the battery will serve an EV immediately after being unloaded from the corresponding CB. Therefore, the FBs cannot be warehoused, which thus deviates from the real operation of some BCSs in practice. In fact, it is the requirement of keeping a dynamic FB inventory with a limited number of CBs that makes the scheduling of BCS challenging: if the loading/unloading action happens very frequently for the purpose of accumulating more FBs in the FB inventory, then the charging control is less flexible since the charging duration of each battery is very short. As a consequence, the charging cost (e.g., the battery degradation cost) will increase. In contrast, if the loading/unloading action happens very slowly for the purpose of reducing charging cost, the FB inventory may not be able to satisfy the FB demand. Therefore, the BCS operator needs to carefully schedule the loading/unloading and charging decisions such that the optimal tradeoff can be achieved. To the best of our knowledge, this tradeoff has not been investigated by all the aforementioned literature.

Motivated by the aforementioned work and the above three important factors of a BCS, this paper tries to propose a general optimization framework for the scheduling of a single BCS. Specifically, we focus on the following BCS scheduling (BCSS) problem: Given the electricity price (e.g., the day-ahead market) and FB demand at known epochs during a fixed time horizon (e.g., a day), how should the BCS operator minimize the total charging cost by controlling the loading/unloading decisions and the charging rates of all CBs to satisfy the FB demand with warehoused FBs in the dynamic FB inventory?

B. Contribution of This Paper

Motivated by the above question, this paper proposes a general optimization framework for the BCSS problem. Meanwhile, we also develop an efficient algorithm for solving the BCSS problem by leveraging its special structural property. In summary, this paper makes the following contributions.

First, we propose to formulate the novel BCSS problem as a mixed-integer program (MIP), in which the binary actions represent the loading/unloading of batteries and the continuous actions denote the batteries' charging rates. Our proposed model considers the fact that the SoC of FBs should exceed a predetermined minimum threshold, the number of CBs is limited, and the FBs should be warehoused in the dynamic FB inventory. To the best of our knowledge, our proposed BCSS problem has not been studied by all the aforementioned

literature. We expect that the proposed model can be a unified framework for many possible future extensions such as integrating renewable energy into the power grid with BCSs, providing ancillary services by the aggregated DBs in the BCS, etc.

Second, we propose an efficient algorithm for solving the BCSS problem. Our proposed BCSS problem is very difficult to be solved directly due to its mixed-integer nature and the strong coupling between binary and continuous decision variables, especially when it is in large scale. Therefore, the second part of this paper focuses on solving the BCSS problem by leveraging its special structural property. Specifically, we observe that the BCSS problem has a highly decomposable structure when fixing the binary decision variables. Therefore, the generalized Benders decomposition (GBD) is applied to solve the BCSS problem in an iterative manner. The salient feature of our algorithm is that the Benders subproblem can be solved efficiently by a highly parallel algorithm.

C. Organization of The Paper

The rest of the paper is organized as follows. We present the details of the system model and formulation of the BCSS problem in Section II. We then present the proposed algorithm in Section III. As the main feature of the proposed algorithm, the decomposable structure of the Benders subproblem and a specifically-designed parallel algorithm are discussed in Section IV. Numerical simulation and discussion are presented in Section V. We finally conclude our paper in Section VI with potential future work.

II. System Model and Problem Formulation

In this section, we introduce the details of the system model and then present the formulation of the BCSS problem.

A. Details of the System Model

As shown in Fig. 1, the system considered in this paper consists of four parts, namely, i) the **power system**, ii) the centralized **BCS**, which further includes the *FB Inventory*, the *DB Inventory*, the *Control Center*, and the *Charging Bays*, iii) the multiple **geographically distributed BSSs**, and iv) the **transportation system**. The BSSs provide battery-swapping service for EVs by first unloading a DB from an EV and then loading a FB into this EV, namely, FBs will be consumed by EVs and DBs will be collected by BSSs. The DBs collected by BSSs will be delivered back to the DB inventory and wait for charging service. Therefore, the batteries (including both DBs and FBs) are circulating between the centralized BCS and multiple geographically distributed BSSs through the transportation system. Note that the power system supplies electricity for the CBs and the Control Center is responsible for all the communication and computation tasks.

Recall that this paper focuses on the BCSS problem, which aims to investigate the optimal charging scheduling of the centralized BCS shown in Fig. 1. In particular, the charging scheduling is performed as follows: a DB will be loaded to one of the CBs if that CB is idle, and then it begins to recharge.

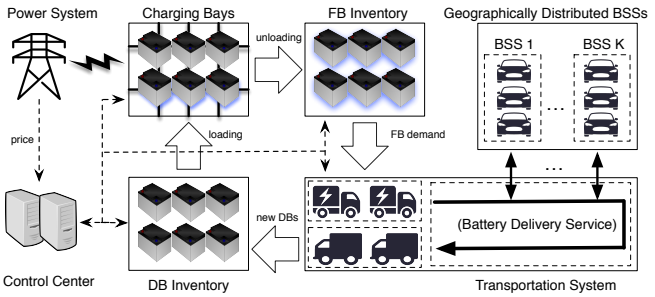

Fig. 1. The system model of a centralized BCS and multiple geographically distributed BSSs. The centralized BCS is comprised of four components: the *FB Inventory*, the *DB Inventory*, the *Control Center*, and the *Charging Bays*.

After being fully-charged, the FB will be unloaded from the corresponding CB and then warehoused in the FB inventory. As we mentioned before, the objective of the BCSS problem is to transform DBs into FBs with the minimum charging cost.

Before leaving this subsection, it is worth pointing out that our proposed BCSS problem is primarily motivated by the scenario when the DB inventory has enough DBs while the initial number of FBs in the FB inventory is not enough to serve the total FB demand. Our model is not suitable for the cases when the FB inventory is full of FBs or equivalently, the DB inventory has very few or no DBs[1], since in these cases the charging scheduling of the BCS becomes less urgent and sometimes even unnecessary. Meanwhile, the specific delivery strategy of DBs and FBs in the transportation system is beyond the scope of this paper. As a rational approximation, we assume that the loading/unloading of batteries in the CBs is instantaneous compared to the long charging time. Meanwhile, it is also practical to assume that both the DB inventory and the FB inventory are capable of warehousing all the batteries available with no capacity constraint.

B. The BCSS Problem

*1) **Individual Constraints on Each CB**:* To denote the operation of *when* to load/unload *which* CB, we introduce a binary decision variable $u_{b,t}$ as

$$u_{b,t} = \{0, 1\}, \forall b \in \mathcal{B}, \forall t \in \mathcal{T} \cup \{T\}. \tag{1}$$

Specifically, when $u_{b,t} = 1$, the battery in CB_b will be unloaded at time t, and a new DB will then be loaded into this CB to start its charging process. Otherwise, when $u_{b,t} = 0$, the current battery will be kept in CB_b for time slot t, and no new DB will be loaded into CB_b. Based on this definition, the SoC of the battery in CB_b at time t, i.e., $s_{b,t}$, evolves as

$$s_{b,t+1} = s_{b,t}(1 - u_{b,t}) + \eta_b r_{b,t} + s_{b,t}^{\mathrm{new}} u_{b,t}, \forall t \in \mathcal{T}, \tag{2}$$

where the charging rate $r_{b,t}$ cannot exceed the power rating:

$$0 \leq r_{b,t} \leq r_b^{\max}, \forall b \in \mathcal{B}, \forall t \in \mathcal{T}. \tag{3}$$

[1]There are two main factors that determine whether or not the DB inventory will have enough DBs most of the time during the scheduling horizon, i.e., i) the initial numbers of FBs and DBs, and ii) the ratio of the number of CBs to the number of EVs. For example, if initially both the FB inventory and the DB inventory have a limited number of batteries, and the ratio of the number of CBs to the number of EVs is very large, then the DB inventory is highly likely to be empty very soon.

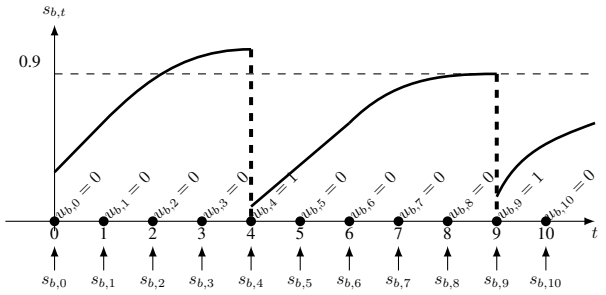

Fig. 2. Illustration of the SoC transitions in CB_b when $\alpha = 0.9$.

Equation (2) indicates that when $u_{b,t} = 1$, the SoC of the battery in CB_b at time t will be initialized to the SoC of the newly loaded DB, namely, $s_{b,t}^{\mathrm{new}}$. Subsequently, the initialized SoC will increase by $\eta_b r_{b,t}$, where η_b denotes the charging efficiency of CB_b. Otherwise, when $u_{b,t} = 0$, the SoC at time $t+1$ is simply equal to the SoC at time t plus $\eta_b r_{b,t}$. Note that in this paper, the SoC of a battery is normalized to be a fraction between 0 and 1. Therefore, $r_{b,t}$ is defined to be the ratio between the charged energy in each time slot and the battery capacity, which denotes the increment of $s_{b,t}$ in fraction instead of the real-charged power (in kW). Note that it is possible to consider the selection of DBs based on their initial SoC as another type of decision variable. However, since $s_{b,t}^{\mathrm{new}}$ is usually small and does not have a significant impact on the total charging time, we thus assume in the same way as [16] that it is known a priori to the BCS operator.[2]

Recall that the SoC of each FB should be larger than or equal to α. We thus have the following constraint:

$$\alpha u_{b,t} \leq s_{b,t} \leq 1, \forall b \in \mathcal{B}, \forall t \in \mathcal{T} \cup \{T\}. \tag{4}$$

Intuitively, inequality (4) guarantees that $s_{b,t}$ is larger than or equal to α at the time when $u_{b,t} = 1$. Otherwise, when $u_{b,t} = 0$, $s_{b,t}$ is simply bounded between 0 and 1. The initial SoCs of all batteries loaded in the CBs at time $t = 0$ are given by

$$s_{b,0} = s_b^{\mathrm{initial}}, \forall b \in \mathcal{B}, \tag{5}$$

where we assume without loss of generality that s_b^{initial} is less than α. Therefore, $u_{b,0} = 0$ holds for all $b \in \mathcal{B}$.

We illustrate the SoC transition of a particular CB in Fig. 2. As can be seen, when $u_{b,4} = u_{b,9} = 1$, the SoC of this CB will be reinitialized. Meanwhile, according to (4), a battery is eligible to be unloaded only when its SoC is larger than or equal to $\alpha = 0.9$; however, the optimal swapping decision highly depends on the objective function. Note that constraints (1)-(5) are defined on each CB level, and we thus call them individual constraints.

*2) **System-Wide Constraints on All CBs**:* In addition to the individual constraints for each CB, we also have two system-wide constraints coupling all the CBs.

[2] In our simulation, we choose $s_{b,t}^{\mathrm{new}}$ randomly from interval $[0, 0.15]$.

- *FB Demand*: We denote the number of FBs at time t by $F_t, \forall t \in \mathcal{T}$, and assume that the initial number of FBs, i.e., F_0, is known a priori. Therefore, we have

$$F_{t+1} = F_t - d_t + \sum_{b=1}^{B} u_{b,t+1}, \forall t \in \mathcal{T}, \tag{6}$$

where $\sum_{b=1}^{B} u_{b,t+1}$ denotes the total number of newly added FBs at time $t+1$. Recall that the total number of FBs at each time $t \in \mathcal{T}$ should be no less than the FB demand d_t,

$$F_t \geq d_t, \forall t \in \mathcal{T} \cup \{T\}. \tag{7}$$

Here, in (7), the additional constraint $F_T \geq d_T$ guarantees that at least d_T FBs will be preserved at the end of the control horizon for future use (i.e., the initial number of FBs for the next scheduling horizon), where d_T is an artificial FB demand determined by the BCS operator beforehand.

- *Transmission Capacity*: For every time slot $t \in \mathcal{T}$, the aggregate charging rate plus the non-battery load L_t should be upper bounded by the transmission capacity C, i.e.,

$$\sum_{b=1}^{B} \frac{\theta r_{b,t}}{\Delta_T} + L_t \leq C, \forall t \in \mathcal{T}, \tag{8}$$

where the battery capacity θ (in kWh) converts $r_{b,t}$ denoted as a fraction (no unit, as defined earlier) to the real-charged energy $\theta r_{b,t}$ (in kWh). Furthermore, $\theta r_{b,t}$ is converted to the real-charged power (in kW) after being divided by Δ_T. Similar to [17], we assume that all the batteries in the BCS have the same capacity. However, the maximum charging rates are allowed to be different.

*3) **Objective of The BCSS Problem**:* The objective of the BCSS problem is to minimize the total charging cost subject to all the aforementioned constraints (1)-(8). The total charging cost includes the electricity purchasing cost (EPC) plus the battery degradation cost (BDC). We assume that the BCS considered here has no market power and is a pure price taker, thus the EPC can be represented by

$$\mathrm{EPC} = \sum_{b=1}^{B} \sum_{t=0}^{T-1} p_t \theta r_{b,t}. \tag{9}$$

Unlike the EPC, the BDC cannot be simply modeled as a linear function of the charging rate. As a typical example of lithium-ion battery technology, $\mathrm{LiFePO_4}$ lithium-ion battery has been widely used in automobile industries [23]. Based on the degradation model of $\mathrm{LiFePO_4}$ lithium-ion battery developed in [23]–[25] and then further developed by [26], the BDC can be expressed as

$$\mathcal{G}_b(r_{b,t}) = a_t r_{b,t}^2 + \sigma_t r_{b,t} + c_t, \tag{10}$$

where parameters a_t, σ_t, and c_t are related to the battery that is being charged at CB_b at time t. Specifically, based on the price of battery cell (\$/kWh) and battery's internal parameters such

as voltage, current, and SoC, all of these three parameters can be determined[3]. Therefore, the total BDC can be calculated as

$$\mathrm{BDC} = \sum_{b=1}^{B} \sum_{t=0}^{T-1} \mathcal{G}_b(r_{b,t}) \tag{11}$$

Therefore, based on the EPC model and the BDC model, the BCSS problem can be formally formulated as the following optimization problem:

$$(\mathrm{BCSS}) \begin{cases} \min \ \mathrm{EPC} + \mathrm{BDC} \\ s.t. \quad (1)-(8), \end{cases} \tag{12}$$

variables: $\{r_{b,t}\}_{\forall b \in \mathcal{B}, \forall t \in \mathcal{T}}, \{u_{b,t}\}_{\forall b \in \mathcal{B}, \forall t \in \mathcal{T} \backslash \{0\} \cup \{T\}}$.

A quick observation for Problem (12) is that all constraints are linear except (2), which consists of multiplication between continuous and binary decision variables. Moreover, from (4) we can see that $u_{b,t} = 1$ is feasible if and only if $\alpha \leq s_{b,t} \leq 1$. Meanwhile, the SoC transition in (2) shows that $s_{b,t}$ depends on $r_{b,t'}$ with $t' \leq t$. Therefore, all the $r_{b,t'}$ with $t' \leq t$ are strongly coupled with $u_{b,t}$. *The mixed-integer nature, the nonlinearity of the SoC transition, and the strong coupling effect between the binary and the continuous decision variables make Problem* (12) *difficult to solve*. The following two sections aim to present a computationally-tractable algorithm to solve Problem (12). Before leaving this section, the following two remarks provide some justification about the generality and feasibility issue of the BCSS problem.

Remark 1 (Generality of the BCSS Problem)**.** *Note that the BCSS problem is a mixed-integer nonlinear program (MINLP). In particular, when we adopt the quadratic BDC model* (11) *for typical* $\mathrm{LiFePO_4}$ *lithium-ion batteries, the BCSS problem becomes a mixed-integer quadratic program (MIQP). Considering the wide application of* $\mathrm{LiFePO_4}$ *in EVs, we focus on the quadratic BDC model* (11) *in this paper and aim to solve the MIQP problem* (12) *hereinafter. However, it is worth pointing out that our BCSS problem can be any general MIP when other nonlinear/linear battery degradation models are introduced or other application scenarios are considered*[4]*. Meanwhile, our proposed algorithm in the following sections is independent of the quadratic BDC model, as long as the objective function of the MINLP problem is convex.*

Remark 2 (Feasibility of the BCSS Problem)**.** *It is possible that the proposed BCSS problem is infeasible if the FB demand is very high. However, we consider that this is a planning problem that should ensure the BCSS problem is feasible before our proposed scheduling problem. For example, the BCS operator has to make a feasible commitment with BSSs such that the total FB demand is within the capability of the BCS, or the BCS operator has to prepare enough FBs such that a given FB demand can be satisfied. Since the planning of a proper BCS is not the focus of this paper, we assume that the BCSS problem is already feasible and focus on the scheduling aspect by proposing an efficient algorithm.*

[3]The detailed expressions for $a_{b,t}, \sigma_{b,t}$, and $c_{b,t}$ are referred to [26].

[4]For instance, in addition to the cost minimization model proposed in Problem (12), the BCS operator can also control the aggregate charging rate of the BCS to provide grid services such as peak-shaving and/or frequency regulation service, etc.

III. An Exact Algorithm based on Generalized Benders Decomposition

In this section, we first show how to transform Problem (12) into a standard MIQP problem. We then propose to solve the MIQP problem with the GBD approach.

A. Standard MIQP Representation

We first represent the nonlinear constraint (2) as equivalent linear constraints. Similar to [27] , for any $b \in \mathcal{B}$ and $t \in \mathcal{T} \cup \{T\}$, we define $y_{b,t} = s_{b,t}(1-u_{b,t})$ as an auxiliary variable and rewrite (2) as

$$s_{b,t+1} = y_{b,t} + \eta_b r_{b,t} + s_{b,t}^{\mathrm{new}} u_{b,t}, t \in \mathcal{T}. \tag{13}$$

To preserve the equivalence between (13) and (2), the auxiliary variable $y_{b,0}$ should be equal to $s_{b,0}$ since $u_{b,0} = 0$ holds for all $b \in \mathcal{B}$. Meanwhile, for all $t \in \mathcal{T} \backslash \{0\} \cup \{T\}$, $y_{b,t}$ must satisfy the following linear inequalities :

$$y_{b,t} \leq y_{b,t-1} + \eta_b r_{b,t-1} + s_{b,t-1}^{\mathrm{new}} u_{b,t-1}, \tag{14a}$$

$$y_{b,t} \geq y_{b,t-1} + \eta_b r_{b,t-1} + s_{b,t-1}^{\mathrm{new}} u_{b,t-1} - u_{b,t}, \tag{14b}$$

$$y_{b,t} \leq 1 - u_{b,t}, \tag{14c}$$

$$y_{b,t} \geq 0. \tag{14d}$$

The equivalence between (13)-(14d) and (2) can be checked as follows: If $u_{b,t} = 0$, constraints (14a) and (14b) guarantee that $y_{b,t} = y_{b,t-1} + \eta_b r_{b,t-1} + s_{b,t-1}^{\mathrm{new}} u_{b,t-1} = s_{b,t} = s_{b,t}(1 - u_{b,t})$, and in this case, constraints (14c) and (14d) are inactive. Otherwise, if $u_{b,t} = 1$, constraints (14c) and (14d) guarantee that $y_{b,t} = 0 = s_{b,t}(1 - u_{b,t})$, and similarly, constraints (14a) and (14b) are inactive. Therefore, constraints (13)-(14d) are indeed equivalent to (2). By utilizing this equivalence, we substitute (13) into constraint (4) and get the following two linear inequality constraints for all $t \in \mathcal{T} \backslash \{0\} \cup \{T\}$:

$$y_{b,t-1} + \eta_b r_{b,t-1} + s_{b,t-1}^{\mathrm{new}} u_{b,t-1} \leq 1, \tag{15a}$$

$$y_{b,t-1} + \eta_b r_{b,t-1} + s_{b,t-1}^{\mathrm{new}} u_{b,t-1} \geq \alpha u_{b,t}. \tag{15b}$$

After the above transformation, (2) and (4) can be equivalently represented by (14a)-(15b). For compactness, we define the following vectors to represent the decision variables: $\mathbf{r}_b^\intercal = \big(r_{b,0}, \cdots, r_{b,T-1}\big), \mathbf{y}_b^\intercal = \big(y_{b,1}, \cdots, y_{b,T}\big)$, and $\mathbf{u}_b^\intercal = (u_{b,1}, \cdots, u_{b,T}), \forall b \in \mathcal{B}$. Thus, the above five linear constraints (14a)-(14c), (15a), and (15b) can be combined into one linear constraint as follows:

$$\mathbf{A}_b \mathbf{r}_b + \mathbf{D}_b \mathbf{y}_b + \mathbf{E}_b \mathbf{u}_b \leq \mathbf{f}_b, \forall b \in \mathcal{B}, \tag{16}$$

where matrices $\{\mathbf{A}_b\}_{\forall b \in \mathcal{B}}$, $\{\mathbf{D}_b\}_{\forall b \in \mathcal{B}}$, and $\{\mathbf{E}_b\}_{\forall b \in \mathcal{B}}$, and vector $\{\mathbf{f}_b\}_{\forall b \in \mathcal{B}}$ can be readily obtained by the corresponding coefficients in (14a)-(14c), (15a), and (15b). Similarly, we can represent constraints (6), (7), and (8) as

$$\sum_{b=1}^{B} \mathbf{G}_b \mathbf{u}_b \geq \mathbf{d}, \quad \sum_{b=1}^{B} \mathbf{r}_b \leq \mathbf{g}, \tag{17}$$

where matrix $\mathbf{G}_b$ consists of only 0 and 1, $\mathbf{d} = (d_t)_{\forall t}$, and $\mathbf{g} = \big(\frac{(C - L_t)\Delta_T}{\theta}\big)_{\forall t}$. Note that the first inequality constraint in (17) corresponds to (6) and (7), and the second one corresponds to (8). Therefore, Problem (12) can be finally represented as a

standard MIQP problem with all linear constraints as follows:

$$\min \sum_{b=1}^{B}\Big[\frac{1}{2}\mathbf{r}_b^\intercal\mathbf{Q}_b\mathbf{r}_b+\mathbf{p}^\intercal\mathbf{r}_b\Big] \tag{18a}$$

$$s.t.\ (16)\text{ and }(17), \tag{18b}$$

$$\mathbf{0}\le\mathbf{r}_b\le\mathbf{r}_b^{\max},\mathbf{y}_b\ge\mathbf{0},\mathbf{u}_b\in\{0,1\}^{T\times 1},\forall b\in\mathcal{B}, \tag{18c}$$

$$\text{variables: }\mathbf{r}_b,\mathbf{y}_b,\mathbf{u}_b,\forall b\in\mathcal{B}, \tag{18d}$$

where $\mathbf{Q}_b$ is a diagonal matrix, $\mathbf{p}$ is the vector compounded by $\theta p_t\Delta_T$ and the linear term in $\mathcal{G}_b(r_{b,t})$, and $\mathbf{r}_b^{\max}$ is a $T\times 1$ vector with all entries equal to $r_b^{\max}$.

After the above representation, Problem (18) can be directly solved by commercial solvers such as Gurobi [34]. However, according to our numerical experiment, the computational time for directly solving Problem (18) with Gurobi 6.5.0 [34] increases significantly even when B is larger than 50 (details will be discussed in Section V). Therefore, instead of directly solving Problem (18) with Gurobi, we will propose a more efficient algorithm by further exploiting the special structure of Problem (18). In particular, similar to [28], the GBD algorithm will be applied here and its details will be presented in the following subsection. Note that in this paper we focus on obtaining the exact solution of Problem (12). Those who are interested in obtaining an approximate solution with commercial solvers are referred to Appendix A.

B. The GBD Algorithm

In GBD, Problem (18) is partitioned into a master problem and a sub-problem. The resulting master problem is solved by a cutting plane algorithm in which, at each iteration, the binary variable of the master problem is first determined and the sub-problem is solved by fixing the binary variable. If the sub-problem is feasible and bounded, an optimality cut is added to the master problem; otherwise a feasibility cut is added. An upper bound can be computed from the feasible sub-problem and a lower bound can be obtained from the master problem. The process continues until an optimal solution is found or the optimality gap is smaller than a given threshold. The whole framework is presented in the following five steps:

`Step-1 (Initialization)`: Select a convergence tolerance parameter $\epsilon\ge 0$. Set $\mathrm{UB}=\infty$ and $\mathrm{LB}=-\infty$. Set the initial cut coefficients $\mathbf{\Phi}_b^1=\hat{\mathbf{\Phi}}_b^1=\mathbf{0}$, and $\Psi_b^1=\hat{\Psi}_b^1=0$, $\forall b\in\mathcal{B}$. Initialize $K=1$ and $L=1$ to count the numbers of optimality constraints and feasibility constraints, respectively.

`Step-2 (Master Problem)`: Solve the following master problem:

$$\min_{\mathbf{u},z}\ z$$

$$s.t.\ \big[\mathbf{\Phi}_1^k,\cdots,\mathbf{\Phi}_B^k\big]\mathbf{u}+\sum_{b=1}^{B}\Psi_b^k\le z,\forall k=1,\cdots,K, \tag{19}$$

$$\big[\hat{\mathbf{\Phi}}_1^\ell,\cdots,\hat{\mathbf{\Phi}}_B^\ell\big]\mathbf{u}+\sum_{b=1}^{B}\hat{\Psi}_b^\ell\le 0,\forall \ell=1,\cdots,L, \tag{20}$$

$$\big[\mathbf{G}_1,\cdots,\mathbf{G}_B\big]\mathbf{u}\ge\mathbf{d},\mathbf{u}\in\{0,1\}^{T\times B}, \tag{21}$$

where $\mathbf{u}^\intercal=(\mathbf{u}_1^\intercal,\cdots,\mathbf{u}_B^\intercal)$. Let $(\mathbf{u}^K,z^K)$ be the optimal solution, and set $\mathrm{LB}=z^K$. Terminate if $\mathrm{UB}\le\mathrm{LB}+\epsilon$.

As will become clear later on, constraint (19) denotes the set of optimality cuts, which will push the lower bound LB closer to the optimal objective value of Problem (18). Meanwhile, constraint (20) represents the set of feasibility cuts, which will make $\mathbf{u}^K$ more feasible for the sub-problem defined in Problem (22). In each iteration, the master problem will have a solution that is greater than or equal to the solution of the previous iteration (i.e., the sequence of LB is non-decreasing). This is because constraints (19) and (20) will keep shrinking the space for searching $\mathbf{u}$ with the increase of K and L.

`Step-3 (Sub-problem)`: Given $\mathbf{u}^K$ from **`Step-2`**, Problem (18) reduces to a continuous optimization problem defined on $\mathbf{r}_b$ and $\mathbf{y}_b,\forall b\in\mathcal{B}$ as follows:

$$F_{\mathrm{sub}}(\mathbf{u}^K)=\min_{\mathbf{r}_b,\mathbf{y}_b}\sum_{b=1}^{B}\Big[\frac{1}{2}\mathbf{r}_b^\intercal\mathbf{Q}_b\mathbf{r}_b+\mathbf{p}^\intercal\mathbf{r}_b\Big] \tag{22a}$$

$$s.t.\ \mathbf{A}_b\mathbf{r}_b+\mathbf{D}_b\mathbf{y}_b\le\mathbf{f}_b-\mathbf{E}_b\mathbf{u}_b^K,\forall b\in\mathcal{B}, \tag{22b}$$

$$\sum_{b=1}^{B}\mathbf{r}_b\le\mathbf{g}, \tag{22c}$$

$$\mathbf{0}\le\mathbf{r}_b\le\mathbf{r}_b^{\max},\mathbf{y}_b\ge\mathbf{0},\forall b\in\mathcal{B}. \tag{22d}$$

Problem (22) is often referred to as the Bender's sub-problem, or sub-problem for short [29], [30]. Determination of whether Problem (22) is feasible or not for a given $\mathbf{u}^K$ can be done by any Phase I algorithm. In particular, Floudas *et al*. in [30] proposed to solve the following linear programming problem:

$$F_{\mathrm{fc}}(\mathbf{u}^K)=\min_{\mathbf{r}_b,\mathbf{y}_b,\boldsymbol{\delta}_b}\sum_{b=1}^{B}\mathbf{e}^\intercal\boldsymbol{\delta}_b \tag{23a}$$

$$s.t.\ \mathbf{A}_b\mathbf{r}_b+\mathbf{D}_b\mathbf{y}_b\le\mathbf{f}_b-\mathbf{E}_b\mathbf{u}_b^K+\boldsymbol{\delta}_b,\forall b\in\mathcal{B}, \tag{23b}$$

$$\sum_{b=1}^{B}\mathbf{r}_b\le\mathbf{g}, \tag{23c}$$

$$\mathbf{0}\le\mathbf{r}_b\le\mathbf{r}_b^{\max},\mathbf{y}_b\ge\mathbf{0},\boldsymbol{\delta}_b\ge 0,\forall b\in\mathcal{B}, \tag{23d}$$

where $\mathbf{e}=(1,1,\cdots,1)^\intercal$. Specifically, the feasibility of the sub-problem can be checked as follows: If $F_{\mathrm{fc}}(\mathbf{u}^K)=0$, $\mathbf{u}^K$ is feasible for the sub-problem. Otherwise, if $F_{\mathrm{fc}}(\mathbf{u}^K)>0$, the sub-problem is infeasible. Depending on the feasibility of the sub-problem, we have the following two steps.

`Step-4 (Optimality Cuts)`: If the sub-problem (22) is feasible, let $\{\mathbf{r}_b^K\}_{\forall b}$ be its optimal primal solution and let $F_{\mathrm{sub}}(\mathbf{u}^K)$ be the optimal objective value. Furthermore, we dualize constraint (22b) with Lagrange multiplier $\{\boldsymbol{\lambda}_b\}_{\forall b}$ and let $\{\boldsymbol{\lambda}_b^K\}_{\forall b}$ be the optimal dual solution. Note that the sub-problem is a convex optimization problem and constraint (22b) is separable in $\mathbf{r}_b$ and $\mathbf{u}_b^K$. Therefore, based on the standard convex optimization theory, $F_{\mathrm{sub}}(\mathbf{u}^K)$ can be given as

$$F_{\mathrm{sub}}(\mathbf{u}^K)=\big[\mathbf{\Phi}_1^{K+1},\cdots,\mathbf{\Phi}_B^{K+1}\big]\mathbf{u}^K+\sum_{b=1}^{B}\Psi_b^{K+1}, \tag{24}$$

where the two coefficients $\mathbf{\Phi}_b^{K+1}$ and Ψ_b^{K+1} are computed based on the optimal primal and dual variables as

$$\mathbf{\Phi}_b^{K+1} = \left\langle \boldsymbol{\lambda}_b^K, \mathbf{E}_b \right\rangle, \forall b \in \mathcal{B}, \tag{25}$$

$$\Psi_b^{K+1} = \frac{1}{2}\left(\mathbf{r}_b^K\right)^\intercal \mathbf{Q}_b \mathbf{r}_b^K + \mathbf{p}^\intercal \mathbf{r}_b^K + \left\langle \boldsymbol{\lambda}_b^K, \mathbf{A}_b \mathbf{r}_b^K + \mathbf{D}_b \mathbf{y}_b^K - \mathbf{f}_b \right\rangle, \forall b \in \mathcal{B}, \tag{26}$$

We store $(\mathbf{u}^K, (\mathbf{r}_b^K)_{\forall b})$ as the incumbent if $F_{\rm sub}(\mathbf{u}^K)$ is less than UB, and update the upper bound $\mathrm{UB} = F_{\rm sub}(\mathbf{u}^K)$. If $\mathrm{UB} \leq \mathrm{LB} + \epsilon$, then we can claim that $(\mathbf{u}^K, (\mathbf{r}_b^K)_{\forall b})$ is the optimal solution for Problem (18) and terminate. Otherwise, increase K by 1 and go to **`Step-2`**.

`Step-5 (Feasibility Cuts)`: If the sub-problem (22) is infeasible, then the feasibility cuts must be added to the master problem. In particular, let $\{\hat{\mathbf{r}}_b^L\}_{\forall b}$, $\{\hat{\mathbf{y}}_b^L\}_{\forall b}$, and $\{\boldsymbol{\delta}_b^L\}_{\forall b}$ be the optimal primal solution for Problem (23), and let $\{\hat{\boldsymbol{\lambda}}_b^L\}_{\forall b}$ be the optimal dual solution associated with constraint (23b). Since Problem (23) is a linear program, its optimal objective value $F_{\rm fc}(\mathbf{u}^K)$ is equivalent to the optimal objective value of its dual problem written as follows:

$$F_{\rm fc}(\mathbf{u}^K) = \left[\hat{\mathbf{\Phi}}_1^{L+1}, \cdots, \hat{\mathbf{\Phi}}_B^{L+1}\right]\mathbf{u}^K + \sum_{b=1}^{B} \hat{\Psi}_b^{L+1}, \tag{27}$$

where the coefficients can be computed as

$$\hat{\mathbf{\Phi}}_b^{L+1} = \left\langle \hat{\boldsymbol{\lambda}}_b^L, \mathbf{E}_b \right\rangle, \forall b \in \mathcal{B}, \tag{28}$$

$$\hat{\Psi}_b^{L+1} = \left\langle \hat{\boldsymbol{\lambda}}_b^L, \mathbf{A}_b \hat{\mathbf{r}}_b^L + \mathbf{D}_b \hat{\mathbf{y}}_b^L - \mathbf{f}_b \right\rangle, \forall b \in \mathcal{B}. \tag{29}$$

After calculating the above two coefficients, increase L by 1 and go to **`Step-2`**.

According to [29], the upper bound UB and the lower bound LB will eventually converge to the same point if the optimal solution is found, or become extremely close to each other if the ϵ-optimal solution is located.[5] It is worth pointing out that after performing the linearization in Section III-A, constraint (22b) is separable between $\mathbf{u}_b^K$ and $\mathbf{r}_b$, and linear in $\mathbf{u}_b^K$. As a result, both the optimality cuts (19) and the feasibility cuts (20) can be expressed as linear functions of $\mathbf{u}_b^K$. Therefore, the master problem remains as a mixed-integer linear programming (MILP) problem (with only one continuous decision variable z). *Transforming the original MIQP problem into a series of MILP problems can significantly save the computational time, as demonstrated by our simulation results in Section V.*

Note that in **`Step-4`**, we need to solve sub-problem (22) to obtain the optimal primal variable $(\mathbf{r}_b^K)_{\forall b}$ as well as solve its dual problem to obtain the optimal dual variable $(\boldsymbol{\lambda}_b^K)_{\forall b}$. Solving both the primal and dual of the sub-problem with generic convex optimization solvers is definitely feasible. However, since we need to iteratively solve the sub-problem, solving this problem in an accurate and efficient way is critical to the overall performance of the GBD method. Therefore, in the next section, we will propose an efficient parallel algorithm for solving the sub-problem.

[5]Note that as we mentioned in **`Step-2`**, the sequence of LB is non-decreasing. However, the sequence of the upper bound UB is not necessarily to be non-increasing. More detailed explanation is referred to in [29].

IV. Solving Sub-Problem (22) in Parallel

In this section, we leverage the special decomposable structure of the BCSS problem and propose an efficient parallel algorithm for solving sub-problem (22). Our parallel algorithm consists of two key procedures: i) the sub-problem is first decomposed into multiple individual sub-problems at each CB level based on dual decomposition (Subsection IV-A), and ii) each individual sub-problem is further partitioned into multiple independent simple optimization problems (Subsection IV-B). However, as some of the constraints are eliminated during the decomposition and partition processes, and thus we further need to synthesize all the required dual variables associated with these constraints for calculating the optimality cuts (Subsection IV-C). Lastly, we will discuss the parallel implementation of our algorithm in Subsection IV-D.

A. Dual Decomposition of the Sub-Problem

Note that if we relax constraint (22c) with Lagrange multiplier $\boldsymbol{\pi}$, then all the CBs are decoupled. Specifically, we have the Lagrange function $\mathbb{L}(\mathbf{r}, \mathbf{y}, \mathbf{u}^K, \boldsymbol{\pi}) = \sum_{b=1}^{B}\sum_{t=0}^{T-1}\left[\mathcal{G}_b(r_{b,t}) + p_t\theta r_{b,t}\Delta_T + \pi_t r_{b,t}\right] - \sum_{t=0}^{T-1}\pi_t g_t$, and thus the dual function can be written as $\mathbb{G}(\boldsymbol{\pi}) = \min_{\mathbf{r},\mathbf{y}} \mathbb{L}(\mathbf{r}, \mathbf{y}, \mathbf{u}^K, \boldsymbol{\pi}) = \sum_{b=1}^{B} S_b(\boldsymbol{\pi}) - \langle \boldsymbol{\pi}, \mathbf{g}\rangle$, where $S_b(\boldsymbol{\pi})$ is the optimal objective value for the following individual sub-problem (**I-Sub**)[6]

$$(\textbf{I-Sub}): \min_{\mathbf{r}_b, \mathbf{y}_b} \sum_{t=0}^{T-1}\left[\mathcal{G}_b(r_{b,t}) + (p_t\theta\Delta_T + \pi_t) r_{b,t}\right]$$

$$\begin{aligned}
s.t.\ & y_{b,t+1} \leq y_{b,t} + \eta_b r_{b,t} + s_{b,t}^{\rm new} u_{b,t}^K, \forall t \in \mathcal{T}, && (\lambda_{1,b,t})\\
& y_{b,t+1} \geq y_{b,t} + \eta_b r_{b,t} + s_{b,t}^{\rm new} u_{b,t}^K - u_{b,t+1}^K, \forall t \in \mathcal{T}, && (\lambda_{2,b,t})\\
& y_{b,t} \leq 1 - u_{b,t}^K, \forall t \in \mathcal{T} \cup \{T\}, && (\lambda_{3,b,t})\\
& y_{b,t} + \eta_b r_{b,t} + s_{b,t}^{\rm new} u_{b,t}^K \leq 1, \forall t \in \mathcal{T} \cup \{T\}, && (\lambda_{4,b,t})\\
& y_{b,t} + \eta_b r_{b,t} + s_{b,t}^{\rm new} u_{b,t}^K \geq \alpha u_{b,t+1}^K, \forall t \in \mathcal{T} \cup \{T\}, && (\lambda_{5,b,t})\\
& 0 \leq r_{b,t} \leq r_b^{\max}, y_{b,t+1} \geq 0, \forall t \in \mathcal{T},
\end{aligned}$$

where the first five constraints correspond to constraint (22b) or equivalently (14a)-(14c) and (15a)-(15b), and the last one constraint corresponds to constraint (22d). Note that $\lambda_{1,b,t}, \cdots, \lambda_{5,b,t}$ are the respective dual variables associated with each corresponding constraint. Meanwhile, these five dual variables are the respective entries of $\boldsymbol{\lambda}_b$ defined in **`Step-4`**, i.e., $\boldsymbol{\lambda}_b = (\lambda_{1,b,t}, \cdots, \lambda_{5,b,t})_{\forall t}$.

The dual problem of the **I-Sub** problem is

$$\max_{\boldsymbol{\pi}} \mathbb{G}(\boldsymbol{\pi}),\ s.t.\ \boldsymbol{\pi} \geq 0, \tag{30}$$

and the update of $\boldsymbol{\pi}$ at iteration n can follow the projected gradient method:

$$\boldsymbol{\pi}(n+1) = \left[\boldsymbol{\pi}(n) + \sigma\left(\sum_{b=1}^{B}\mathbf{r}_b(n) - \mathbf{g}\right)\right]^+. \tag{31}$$

Since the **I-Sub** problem is a convex optimization problem, the Lagrange multiplier $\boldsymbol{\pi}$ is guaranteed to converge to the optimal solution, as long as the step-size σ is sufficiently small.

[6]By individual, we mean this optimization problem is defined at each individual CB level.

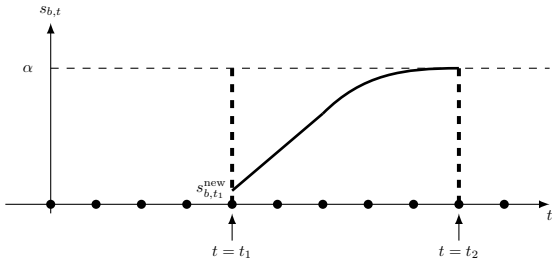

Fig. 3. Illustration of one charging cycle between t_1 and t_2.

B. Partition of the *I-Sub* Problem and Its Equivalent Form

Once $\mathbf{u}^K$ is given, the **I-Sub** problem can be automatically decomposed into a series of smaller optimization problems defined on different charging cycles. For instance, Fig. 3 illustrates one charging cycle that starts from $t = t_1$ and finishes at $t = t_2$, where t_1 and t_2 are two consecutive time instants with $u^K_{b,t_1} = u^K_{b,t_2} = 1$. Intuitively, the **I-Sub** problem defined within $[t_1, t_2)$ is completely independent of the **I-Sub** problem defined within other charging cycles. For a given $\boldsymbol{\pi}(n)$ at iteration n, the **I-Sub** problem defined within the charging cycle exemplified in Fig. 3 can be written as

$$(\textbf{OC-I-Sub}): \min \sum_{t=t_1}^{t_2-1} \Big[\mathcal{G}_b(r_{b,t}) + \big(p_t\theta\Delta_T + \pi_t(n)\big) r_{b,t}\Big]$$

$$s.t.\ s^{\text{new}}_{b,t_1} + \sum_{t=t_1}^{t_2-1} \eta_b r_{b,t} = \alpha, \qquad (\beta_{b,t_1}) \tag{32a}$$

$$0 \le r_{b,t} \le r^{\max}_b, \forall t \in \{t_1, \cdots, t_2 - 1\}, \tag{32b}$$

where β_{b,t_1} in the parentheses of (32a) denotes the dual variable associated with the equality constraint.[7] We refer to the above optimization problem as the one-cycle **I-Sub** (**OC-I-Sub**) problem since it is defined within only one charging cycle.

Note that when $t \in [t_1, t_2)$, the **OC-I-Sub** problem is equivalent to the **I-Sub** problem but contains fewer constraints and variables. Therefore, it is more efficient to solve the **OC-I-Sub** problem instead of solving the **I-Sub** problem. By updating $\boldsymbol{\pi}$ according to (31) and solving the **OC-I-Sub** problem for all charging cycles in an iterative manner, we can obtain the optimal charging rate $\{\mathbf{r}^K_b\}_{\forall b}$, which is required by **`Step-4`** in the GBD algorithm. However, since the auxiliary decision variable $\{\mathbf{y}_b\}_{\forall b}$ is eliminated in the **OC-I-Sub** problem, we thus need to reproduce its optimal value $\{\mathbf{y}^K_b\}_{\forall b}$ based on $\{\mathbf{r}^K_b\}_{\forall b}$. Note that this is a light-weight task since we only need to perform some basic linear algebraic calculations based on the SoC transition equation (2) and the equation $y^K_{b,t} = s^K_{b,t}(1 - u^K_{b,t}), \forall b \in \mathcal{B}$.

[7]Note that $r_{b,t}$ is always non-negative (i.e., no discharging is allowed) and the objective function of the **I-Sub** problem is monotonic in $r_{b,t}$. Therefore, the constraint dualized by $\lambda_{5,b,t}$ in the **I-Sub** problem must be binding if $u^K_{b,t+1} = 1, \forall t \in \mathcal{T}$. As a result, once $\mathbf{u}^K_b$ is given, we can represent the first five constraints in the **I-Sub** problem as an equality constraint shown in (32a).

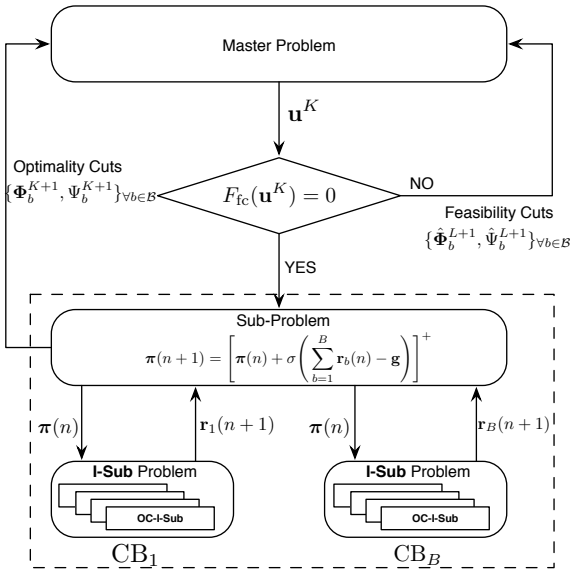

Fig. 4. Illustration of the the GBD with dual decomposition and partition.

C. Synthesis of $\boldsymbol{\lambda}^K$ for Calculating the Optimality Cuts

In the above two subsections, we already obtained the optimal primal variables $\{\mathbf{r}^K_b\}_{\forall b}$ and $\{\mathbf{y}^K_b\}_{\forall b}$ for sub-problem (22). However, in order to calculate the optimality cuts in (25) and (26), we also need the optimal dual variable $\{\boldsymbol{\lambda}^K_b\}_{\forall b}$. Unfortunately, solving the dual of the **OC-I-Sub** problem can only give the dual variable $\{\beta^K_{b,t_1}\}_{\forall b}$ for the charging cycle within $[t_1, t_2)$. Therefore, we further need to synthesize $\{\boldsymbol{\lambda}^K_b\}_{\forall b}$ from $\{\beta^K_{b,t_1}\}_{\forall b}$.

Recall that $\boldsymbol{\lambda}^K_b = (\lambda^K_{1,b,t}, \cdots, \lambda^K_{5,b,t})_{\forall t}$. Based on the relationship between the **I-Sub** problem and the **OC-I-Sub** problem, we can synthesize the detailed entries of $\boldsymbol{\lambda}^K_b$ as follows:

- $\lambda^K_{1,b,t}$ and $\lambda^K_{2,b,t}$ can be any non-negative solution that satisfies $\lambda^K_{1,b,t} - \lambda^K_{2,b,t} = \beta^K_{b,t_1} \cdot \mathbb{I}_{\{u^K_{b,t+1}=0\}}$, $\forall t \in \{t_1, \cdots, t_2 - 1\}$.
- $\lambda^K_{3,b,t} = \beta^K_{b,t_1} \cdot \mathbb{I}_{\{u^K_{b,t}=1\}}, \forall t \in \{t_1, \cdots, t_2 - 1\}$.
- $\lambda^K_{4,b,t} = 0, \forall t \in \{t_1, \cdots, t_2 - 1\}$.
- $\lambda^K_{5,b,t} = \beta^K_{b,t_1} \cdot \mathbb{I}_{\{u^K_{b,t+1}=1\}}, \forall t \in \{t_1, \cdots, t_2 - 1\}$.

Here, we only show the synthesis within the charging cycle $[t_1, t_2)$ exemplified in Fig. 3, and omit the other charging cycles due to their similarity. The correctness of the above synthesis is shown in Appendix B.

D. Algorithm Illustration and Parallel Implementation

We illustrate the GBD algorithm with dual decomposition and the partition manipulation in Fig. 4. Note that the **I-Sub** problems can be solved in parallel among all the CBs. Moreover, the multiple **OC-I-Sub** problems corresponding to each **I-Sub** problem can also be solved in parallel. Therefore, given $\boldsymbol{\pi}(n)$ at iteration n, calculating the dual function in (30) reduces to solving multiple independent **OC-I-Sub** problems in a highly parallel fashion.

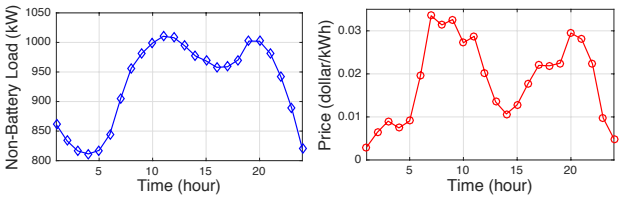

(a) Non-battery load. (b) Electricity price.

Fig. 5. The non-battery load and electricity price in 1-hour granularity.

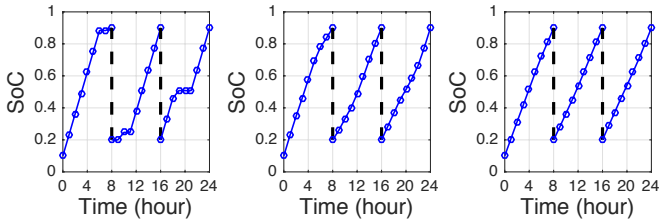

(a) $a = 0$ (b) $a = 5$ (c) $a = 10$

Fig. 6. Comparison between the optimal charging profiles when battery degradation cost increases from the leftmost figure to the rightmost figure.

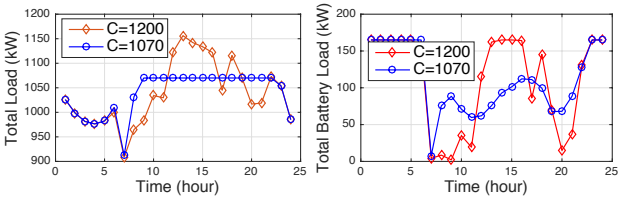

(a) Total load. (b) Total battery load.

Fig. 7. Illustration of the total load and the total battery load with different transmission capacities.

V. Simulation Results

In this section, we validate our optimization model and algorithm with real data simulation. We focus on a one-day scheduling horizon with one hour per slot. We assume $\mathcal{G}_b(r_b, t) = ar_{b,t}^2$, where coefficient $a = 5$ unless otherwise specified[8]. The non-battery load L_t and the day-ahead electricity price p_t are from NYISO [32], and are plotted in Fig. 5. The parameters of the BCS are listed in Table I, where the battery parameters are from the Nissan Leaf [33]. As we mentioned before, the initial SoC for all CBs and the SoC for all newly loaded DBs are randomly drawn from $[0, 0.15]$. Meanwhile, as listed in Table I, $F_0 = 50$. For the FB demand, we set $d_6 = d_{14} = d_{20} = 50$ and $d_t = 0$ for $t \in \mathcal{T}\backslash\{6, 14, 20\}$. Furthermore, we set $d_T = 50$, which guarantees that at least 50 FBs will be preserved as the initial number of FBs for the following scheduling horizon. We solve the master problem via Gurobi 6.5.0 [34] and solve the **OC-I-Sub** problem via CVX 2.1 [35]. To implement our proposed algorithm in parallel, we leverage the embedded `parfor` function of the MATLAB Parallel Computing Toolbox [36]. All the algorithms in this paper are implemented in MATLAB R2015a on an Intel Core i7-4770K Haswell 3.5GHz CPU, 16G RAM PC.

TABLE I
Parameters of the BCS

Parameters	Values
Battery Capacity θ	24 kWh
Charging Efficiency η_b	0.9
Power Rating $r_b^{\max}$	3.3 kW
Threshold α	0.9[9]
Initial Number of FBs F_0	50
Number of CBs B	50

*1) **Impact of Battery Degradation on Charging Smoothness**:* We first show the impact of the batteries' degradation cost on the charging strategy. Specifically, in Fig. 6(a), we set $a = 0$, which means that the battery degradation cost is neglected. In this case, the charging profile is completely influenced by the price fluctuation. Therefore, the charging profiles in Fig. 6(a) shows a rapid fluctuation. In comparison, when the battery degradation cost is taken into account, the optimal charging strategy tends to be much smoother, as shown in Fig. 6(b). Meanwhile, following our intuition, the charging profile becomes almost linear if the battery degradation cost is very high, as shown in Fig. 6(c). Therefore, if the batteries's capital cost is very high, the BCS operator does not need to adjust the charging rate of each CB to exploit the price fluctuation. In contrast, with the decreasing of the batteries' capital cost in the future, the BCS operator will have better opportunities in the dynamic electricity market. Note that the optimal decision is to always swap out the FB once it reaches the minimum SOC threshold $\alpha = 0.9$.

*2) **Impact of Transmission Capacity on Charging Behavior**:* Fig. 7 illustrates the impact of the transmission capacity on the total load and the total battery load. As we can see from Fig. 7(a), the maximum total load is strictly upper bounded by the transmission capacity $C = 1070$ kW during time interval $[9, 22]$. As a result, the total battery load is still high during time interval $[8, 11]$ even though the electricity price around this period is high, as shown by the curve with circles in Fig. 7(b). In comparison, when the transmission capacity is always enough to support all the CBs, as shown by the curve with diamonds in Fig. 7(b), the optimal charging strategy shifts the battery load in $[8, 11]$ to time interval $[12, 16]$, which thus reduces the total charging cost by exploiting the low price (see Fig. 5(b)). Therefore, the transmission capacity can greatly determine the BCS operator's capability of exploiting the price fluctuations.

*3) **Sensitivity Analysis of the Charging Cost to C and B**:* To further show the impact of the transmission capacity on the total cost, we calculate the optimal total cost when the transmission capacity varies from $C = 1100$ kW to $C = 1200$ kW with B set to 50. As we can see from Fig. 8(a), the total cost decreases from 37.9 dollars when $C = 1100$ to 36.1 dollars when $C \geq 1180$. Therefore, increasing the transmission capacity by 80 kW can bring 5% reduction in

[8]The calculation of the exact BDC function is referred to [24] and [26]. Here in our simulation $a = 5$ roughly means the price of battery cell is around \$430 per kWh for all the batteries. However, it should be noted that the average price of battery cell is falling every year [31].

[9]The usable capacity of the Nissan Leaf is around 21.3 kWh according to [33], and thus α is roughly around 0.9.

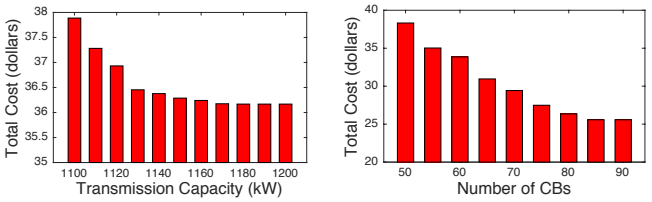

(a) $B = 50$ (b) $C = 1070$ kW

Fig. 8. Impact of C and B on the total cost.

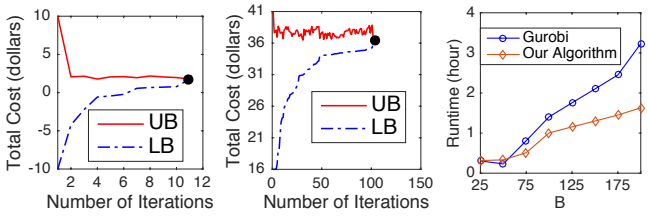

(a) $B = 10$. (b) $B = 50$. (c) CPU Time.

Fig. 9. Convergence and CPU time of the proposed algorithm.

the total cost. In addition to the transmission capacity, another important parameter for the BCS is the total number of CBs, i.e., the value of B. It is intuitive that the charging cost will decrease if we have more CBs. However, what remains unclear is how sensitive the charging cost is to the value of B. Therefore, we plot the optimal charging costs of the BCS when B varies from 50 to 90 with C set to 1070 kW in Figure 8(b). As we can see, the charging cost decreases from 38.32 dollars when $B = 50$ to 25.58 dollars when $B \geq 85$, which demonstrates over 33% improvement.

Based on the comparison between Fig. 8(a) and Fig. 8(b), it is clear that the charging cost is much more sensitive to B than to C. However, it is incorrect to claim that it is always more beneficial to have more CBs than to have higher transmission capacity. This is because the net improvement of the charging cost heavily relies on the marginal costs of increasing C and B. In practice, the marginal cost of increasing C is complex, and is related to the capital cost of the transmission cable, the locational marginal price obtained from the underlying optimal power flow problem, etc. In comparison, the marginal cost of increasing B is relatively simpler and depends only on the infrastructure cost (chargers and cables, etc.). In summary, to reduce the charging cost, it requires a careful calculation before making any further investment on whether to increase B or C.

*4) **Convergence and Efficiency Illustration**:* Fig. 9 demonstrates the convergence and efficiency of our proposed decomposition algorithm. As shown in Fig. 9(a), when $B = 10$, our algorithm converges to the optimality in 11 iterations. Fig. 9(b) shows that when $B = 50$, our algorithm needs around 100 iterations to achieve the ϵ-optimality, where we set $\epsilon = 10^{-3}$. Note that the sequence of LB is always non-decreasing. This is because the master problem is a minimization problem and in each iteration, one extra constraint will be added to the master problem no matter whether the sub-problem is feasible or not. In comparison, Benders decomposition does not guarantee that the sequence of UB has a similar monotonic property, and this can be observed from Fig. 9(a) and (b) that the sequences of UB are indeed not monotonic. However, the sequence of the updated upper bounds UB can be forced to be monotonically non-increasing as long as we always keep the lowest upper bound. It should be noted that the convergence of the algorithm will be the same no matter whether the update of UB is forced to be monotonic or not [29], [30]. To show the scalability of our proposed algorithm, Fig. 9(c) shows the runtime comparison between our proposed algorithm and Gurobi in solving large-scale BCSS problems. As shown in Fig. 9(c), when $B = 25$ and $B = 50$, the runtimes of Gurobi and our proposed algorithm are almost the same. However, our proposed algorithm outperforms Gurobi when $B > 50$. In particular, when $B = 200$, our proposed algorithm reduces the runtime of Gurobi by almost a half.

Based on our computational experiment, we observe that if the coupling effects between binary variables and continuous variables are very strong, and the Benders subproblem happens to have very good and special properties (e.g., partially or fully separable, analytical solution, etc.), then it is highly likely that the algorithm will be very efficient. Our BCSS problem is exactly like this case. Once the binary variables are fixed, the Benders subproblem can be decomposed into multiple identically-structured individual subproblems, namely the one-cycle individual subproblem (**OC-I-Sub**) illustrated in Fig. 3. In summary, it is the strong separability of the Benders subproblem and the parallel computation that ensure the efficiency of our algorithm, as demonstrated in Fig. 9.

VI. Conclusion and Future Work

This paper has studied the BCSS problem, whose main task is to find the cost-minimal scheduling strategy such that the FB inventory can satisfy the FB demand. We formulate the BCSS problem as an mixed-integer program and then solve this problem by the GBD algorithm. The salience of the proposed algorithm is that i) each charging bay can solve its own subproblem in a parallel fashion, and ii) each subproblem can be further decomposed into multiple independent quadratic programming problems, and thus the algorithm facilitates an efficient parallel implementation. Real data simulation has been presented to validate the proposed model and demonstrates the efficiency of the proposed algorithm.

The investigated BCSS problem can be extended in many directions in future. For instance, when there exist multiple geographically-distributed BCSs, how to perform the joint optimization of the high-level charging scheduling and the bottom-level optimal power flow problem is an interesting question. Moreover, battery-to-grid service (via discharging) is a very important application that has not been discussed in this paper.

Appendix A
An Approximate Solution

We note that for general applications in industry, large-scale MINLP models are often approximated and optimized as MILP problems for commercial solvers, e.g., CPLEX, Gurobi.

TABLE II
PERFORMANCE COMPARISON BETWEEN MIQP AND MILP

B	MIQP Model		MILP Model	
	Cost ($)	CPU Time (sec.)	Cost ($)	CPU Time (sec.)
50	38.32	1391.4	40.12	60.6
60	33.86	3124.5	35.29	94.4
70	29.43	4227.6	30.91	173.9
80	26.35	6644.4	27.93	240.8
90	25.58	7544.1	27.18	400.3

Towards this end, in this appendix, we propose an approximate MILP model for the BCSS problem. According to our simulation, the approximation here facilitates a computational-tractable MILP model with acceptable solution for practical systems. Specifically, according to Jensen's inequality, we have

$$\text{BDC} = \sum_{b=1}^{B}\sum_{t=0}^{T-1}\Big(a_t r_{b,t}^2 + \sigma_t r_{b,t} + c_t\Big) \tag{33}$$

$$\geq \sum_{t=0}^{T-1}\frac{a_t R_t^2}{B} + \sum_{t=0}^{T-1}\sigma_t R_t + \sum_{t=0}^{T-1} B c_t, \tag{34}$$

where R_t is the aggregate charging rate defined as

$$R_t \triangleq \sum_{b=1}^{B} r_{b,t}, \tag{35}$$

and the equality in (34) is achieved when $r_{b,t} = r_{b',t}$ for all $b, b' \in \mathcal{B}$, $\forall t \in \mathcal{T}$. Considering the fact that most of the DBs are close to be empty and CBs tend to be homogeneous, it is thus reasonable to approximate the objective of Problem (12) by $f(\mathbf{R})$ as follows

$$f(\mathbf{R}) = \sum_{t=0}^{T-1}\left(\frac{a_t R_t^2}{B} + \Big(p_t\theta + \sigma_t\Big)R_t + Bc_t\right), \tag{36}$$

where $\mathbf{R} = (R_t)_{t=0}^{T-1}$. Therefore, we get the approximate version of the BCSS problem, which we call it as BCSS-A, as follows:

$$\text{(BCSS-A)}\ \ \min\ f(\mathbf{R})\ s.t.\ (1)-(8),\ \text{and}\ (35).$$

The BCSS-A problem facilitates a computationally-tractable MILP model when we further approximate $f(\mathbf{R})$ as a piecewise linear (PWL) cost function. Note that the objective of the BCSS problem has $B \times T$ quadratic terms while $f(\mathbf{R})$ only involves T quadratic terms. Therefore, we can significantly reduce the number of auxiliary variables when we implement the PWL objective in commercial solvers such as Gurobi[10].

We compare both the cost and computational performance of the MIQP model and the approximate MILP model in Table II[11]. Specifically, we choose the same parameter setting as Fig. 8(b) and vary B from 50 to 90 to gradually increase the scale of the system. Both the MIQP model and the approximate MILP model are solved by Gurobi 6.5.0 in MATLAB R2015a on an Intel Core i7-4770K Haswell 3.5GHz CPU, 16G RAM PC. In particular, the PWL objective in the approximate MILP model is implemented by the built-in PWL objective support in Gurobi 6.5.0 with 20 line segments. As shown by Table II, the cost performance of the approximate MILP model is close to the exact MIQP model (less than 6.5% gap). However, the CPU time of solving the approximate MILP model is significantly less than that of the MIQP model.

Note that the performance of our proposed approximate MILP model can be affected by many factors such as the heterogeneity of batteries and the tightness of the transmission capacity (larger C means less coupling among CBs, and thus the performance of the approximate MILP model becomes better, and vise versa.). Therefore, the approximate MILP model in this appendix just serves as a proof of concept for applying approximation techniques to our BCSS problem.

[10] There exist multiple suitable techniques such as Special Ordered Sets of Type Two (SOS2) to implement the PWL objective. Some commercial solvers have built-in PWL objective and constraints support (e.g., Gurobi 6.5.0 [34]).

[11] Note that the cost performance of the approximate MILP model is not its objective value. Instead, it is the real charging cost (including both EPC and BDC) by substituting the charging scheduling results obtained from the approximate MILP model into the objective of the original BCSS problem.

APPENDIX B
SYNTHESIS OF THE DUAL VARIABLE

The **OC-I-Sub** problem is equivalent to the following optimization problem if we relax constraint (32a) with the optimal multiplier β_{b,t_1}^K:

$$\min \quad \sum_{t=t_1}^{t_2-1}\Big[\mathcal{G}_b(r_{b,t}) + \big(p_t\theta\Delta_T + \pi_t(n)\big)r_{b,t}\Big] - \sum_{t=t_1}^{t_2-1}\beta_{b,t_1}^K\eta_b r_{b,t} + \beta_{b,t_1}^K(\alpha - s_{b,t_1}^{\text{new}}) \tag{37a}$$

$$s.t. \quad 0 \leq r_{b,t} \leq r_b^{\max}, \forall t \in \{t_1, \cdots, t_2-1\}. \tag{37b}$$

Similarly, Problem **I-Sub** is equivalent to the following optimization problem if we relax its first five and the last constraints with their respective optimal multipliers:

$$\begin{aligned}\min \quad & \sum_{t=t_1}^{t_2-1}\Big[\mathcal{G}_b(r_{b,t}) + (p_t\theta\Delta_T + \pi_t)r_{b,t}\Big] + \\ & (\lambda_{1,b,t_1}^K - \lambda_{2,b,t_1}^K)\big(y_{b,t_1+1} - y_{b,t_1} - \eta_b r_{b,t_1} - s_{b,t_1}^{\text{new}}\big) + \\ & \sum_{t=t_1+1}^{t_2-2}(\lambda_{1,b,t}^K - \lambda_{2,b,t}^K)\big(y_{b,t+1} - y_{b,t} - \eta_b r_{b,t}\big) + \\ & \lambda_{3,b,t_1}^K y_{b,t_1} - \lambda_{5,b,t_2-1}^K\big(y_{b,t_2-1} + \eta_b r_{b,t_2-1} - \alpha\big) \\ & - \sum_{t=t_1}^{t_2-1}\gamma_{b,t+1}^K y_{b,t+1}\end{aligned} \tag{38a}$$

$$s.t. \quad 0 \leq r_{b,t} \leq r_b^{\max}, \forall t \in \{t_1, \cdots, t_2-1\}, \tag{38b}$$

where $\gamma_{b,t+1}^K$ denotes the optimal multiplier associated with the last constraint of Problem **I-Sub**. Note that we eliminate the constraint associated with $\lambda_{4,b,t}^K$ since $\lambda_{4,b,t}^K = 0$ always holds. We can also eliminate the last term in (38a) since $\sum_{t=t_1}^{t_2-1}\gamma_{b,t+1}^K y_{b,t+1} = 0$ always holds. Let us temporarily

ignore the first term in (38a) and rearrange the order of the remaining terms as

$$\lambda^K_{3,b,t_1} y_{b,t_1} + (\lambda^K_{1,b,t_1} - \lambda^K_{2,b,t_1})\big(y_{b,t_1+1} - y_{b,t_1}\big) + \sum_{t=t_1+1}^{t_2-2} (\lambda^K_{1,b,t} - \lambda^K_{2,b,t})\big(y_{b,t+1} - y_{b,t}\big) - \lambda^K_{5,b,t_2-1} y_{b,t_2-1} - (\lambda^K_{1,b,t_1} - \lambda^K_{2,b,t_1})\eta_b r_{b,t_1} - \sum_{t=t_1+1}^{t_2-2} (\lambda^K_{1,b,t} - \lambda^K_{2,b,t})\eta_b r_{b,t} - \lambda^K_{5,b,t_2-1}\eta_b r_{b,t_2-1} + \lambda^K_{5,b,t_2-1}\alpha - (\lambda^K_{1,b,t_1} - \lambda^K_{2,b,t_1}) s^{\text{new}}_{b,t_1}. \tag{39}$$

Note that if $\lambda^K_{1,b,t} - \lambda^K_{2,b,t} = \lambda^K_{3,b,t_1} = \lambda^K_{5,b,t_2-1} = \beta^K_{b,t_1}$, $\forall t \in \{t_1, \cdots, t_2 - 2\}$, (39) can be equivalently simplified to the following formula

$$-\sum_{t=t_1}^{t_2-1} \beta^K_{b,t_1}\eta_b r_{b,t} + \beta^K_{b,t_1}(\alpha - s^{\text{new}}_{b,t_1}), \tag{40}$$

which is the same as the last two terms in the objective function of Problem (37). Therefore, the optimal dual variable $\boldsymbol{\lambda}^K_b$ can indeed be synthesized according to the following method:

- $\lambda^K_{1,b,t}$ and $\lambda^K_{2,b,t}$ can be any non-negative solution that satisfies $\lambda^K_{1,b,t} - \lambda^K_{2,b,t} = \beta^K_{b,t_1} \cdot \mathbb{I}_{\{u^K_{b,t+1}=0\}}$, $\forall t \in \{t_1, \cdots, t_2 - 1\}$.
- $\lambda^K_{3,b,t} = \beta^K_{b,t_1} \cdot \mathbb{I}_{\{u^K_{b,t}=1\}}$, $\forall t \in \{t_1, \cdots, t_2 - 1\}$.
- $\lambda^K_{4,b,t} = 0$, $\forall t \in \{t_1, \cdots, t_2 - 1\}$.
- $\lambda^K_{5,b,t} = \beta^K_{b,t_1} \cdot \mathbb{I}_{\{u^K_{b,t+1}=1\}}$, $\forall t \in \{t_1, \cdots, t_2 - 1\}$.

For other charging cycles, e.g., a charging cycle that starts from $t = t'_1$ and ends at $t = t'_2$, we will obtain another optimal dual variable β^K_{b,t'_1}, and the the same approach can be applied to synthesize $\boldsymbol{\lambda}^K_b$ within this charging cycle. After visiting all the charging cycles, all the entries of $\boldsymbol{\lambda}^K_b$ can be synthesized.

REFERENCES

[1] E. Ungar and K. Fell, "Plug in, turn on, and load up," *IEEE Power Energy Mag.*, vol. 8, no. 3, pp. 30-35, May.-Jun., 2010.

[2] M. Yilmaz and P.T. Krein, "Review of battery charger topologies, charging power levels, and infrastructure for plug-in electric and hybrid vehicles," *IEEE Trans. Power Electron.*, vol.28, no. 5, pp. 2151-2169, 2012.

[3] Battery Swapping Project for Electric Buses in Qingdao, China. [Online]. Available: http://www.electronicsnews.com.au/features/battery-swapping-becoming-common-practice-for-comm.

[4] J. Kim, I. Song, and W. Choi, "An electric bus with a battery exchange system," *Energies*, vol 8, no. 7, pp. 6806-6819, July 2015.

[5] A. Kuperman, U. Levy, J. Goren, A. Zafransky, and A. Savernin, "Battery charger for electric vehicle traction battery switch station, *IEEE Trans. Ind. Electron.*, vol. 60, no. 12, pp. 5391-5399, Dec. 2013.

[6] [Online]. Available: http://www.technologyreview.com/news/516276/why-tesla-thinks-it-can-make-battery-swapping-work/

[7] H. Mak, Y. Rong, and Z.M. Shen, "Infrastructure planning for electric vehicles with battery swapping," *Management Science*, vol. 59, no. 7, pp. 1557-1575, July 2013.

[8] Y. Miao, Q. Jiang, and Y. Cao, "Battery switch station modeling and its economic evaluation in microgrid," *IEEE PES General Meeting*, 2012.

[9] M. Takagi, Y. Iwafune, H. Yamamoto, K. Yamaji, K. Okano, R. Hiwatari, and T. Ikeya, "Economic value of PV energy storage using batteries of battery switch stations, *IEEE Trans. Sust. Energy*, vol. 4, no. 1, pp. 164-173, Jan. 2013.

[10] P. Lombardi, M. Heuer, Z. Styczynski. "Battery switch station as storage system in an autonomous power system: Optimization issue," *IEEE PES General Meeting*, 2010.

[11] B. Avci, K. Girotra, and S. Netessine, "Electric vehicles with a battery switching station: adoption and environmental impact," *Management Science*, vol. 61, no. 4, pp. 772-794, April 2015.

[12] L. Cheng, Y. Chang, J. Lin and C. Singh, "Power system reliability assessment with electric vehicle integration using battery exchange mode," *IEEE Trans. Sustainable Energy*, vol. 4, No. 4, Oct. 2013.

[13] Y. Zheng, Z. Dong, Y. Xu, K. Meng, J. Zhao and J. Qiu, "Electric vehicle battery charging/swap stations in distribution systems: Comparison study and optimal planning," *IEEE Trans. Power System*, vol. 29, no. 1, 2014.

[14] B. Sun, X. Tan and D.H.K Tsang, "Optimal operation of BSSs with QoS guarantee," *IEEE SmartGridComm 2014*, Venice, Italy, Nov. 2014.

[15] S. Nurre, R. Bent, F. Pan, T. Sharkey, "Managing operations of plug-in hybrid electric vehicle (PHEV) exchange stations for use with a smart grid". *Energy Policy*, vol. 67, pp. 364-377, April 2014.

[16] M. Sarker, H. Pandžić, M. Ortega-Vazquez, "Optimal operation and services scheduling for an electric vehicle battery swapping station," *IEEE Trans. Power Syst.*, vol. 30, no. 2, pp. 901-910, July 2015.

[17] P. You, Z. Yang, Y. Zhang, S. Low, Y. Sun, "Optimal charging schedule for a battery switching station serving electric buses," *IEEE Trans. Power Systems*, vol. 31, no. 5, pp. 3473-3483, Sept. 2016.

[18] R. Widrick, S. Nurre, and M. Robbins, "Optimal policies for the management of an electric vehicle battery swap station," to appear in *Transp. Sci.*, 2016.

[19] O. Worley and D. Klabjan, "Optimization of battery charging an purchasing at electric vehicle battery swap stations," *in Proc. 2011 IEEE Vehicle Power and Propulsion Conf.*, pp. 1-4, 2011.

[20] T. Raviv, "The battery switching station scheduling problem," *Operations Research Letters*, vol. 40, no. 6, pp. 546-550, June 2012.

[21] B. Sun, Zhe Huang, X. Tan, and D.H.K. Tsang, "Optimal scheduling for electric vehicle charging with discrete charging levels in distribution grid," accepted by *IEEE Transactions on Smart Grid*, 2016.

[22] I. Dincer, H.S. Hamut, N. Javani, "Thermal Management of Electric Vehicle Battery Systems," *Automotive Series, Wiley*, 2017.

[23] J. Forman, J. Stein, H. Fathy, "Optimization of dynamic battery parameter characterization experiments via differential evolution," *in proceedings of American Control Conference*, pp. 867-874, Washington, DC, USA, 2013.

[24] J. Forman, S. Moura, J. Stein, H. Fathy, "Optimal experimental design for modeling battery degradation," *in Proceedings of Dynamic Systems and Control Conference*, pp. 309318, 2012.

[25] S. Moura, J. Forman, S. Bashash, J. Stein, H. Fathy, "Optimal control of film growth in lithium-ion battery packs via relay switches," *IEEE Trans. Industrial Electronics*, vol. 58, no. 8, pp. 3555-3566, 2011.

[26] Z. Ma, S. Zou, L. Ran, X. Shi and I.A. Hiskens, "Efficient decentralized coordination of large-scale plug-in electric vehicle charging," *Automatica*, vol. 69, pp. 35-47, 2016.

[27] C. P. Christelle and M. Sevaux, *Applications of optimization with XpressMP*, 2002.

[28] Z. Yang, K. Long, P. You, and M.Y. Chow, "Joint Scheduling of Large-Scale Appliances and Batteries via Distributed Mixed Optimization," IEEE Trans. Power Systems, vol. 30, no. 4, pp. 2031-2040, Jul. 2015.

[29] A. Geoffrion, "Generalized benders decomposition," *Journal of Optimization Theory and Applications*, vol. 10, no. 4, pp. 237-260, 1972.

[30] C. Floudas, A. Aggarwal, and A. Ciric, "Global optimum search for nonconvex NLP and MINLP problems," *Computers and Chemical Engineering*, no. 10, pp. 1117-1132, 1989.

[31] [Online]. Available: https://electrek.co/2017/01/30/electric-vehicle-battery-cost-dropped-80-6-years-227kwh-tesla-190kwh/.

[32] [Online]. Available: http://www.nyiso.com/public/markets_operations/market_data/pricing_data/index.jsp.

[33] [Online]. Available: https://en.wikipedia.org/wiki/Nissan_Leaf.

[34] Gurobi Optimization. [Online]. Available: http://www.gurobi.com/

[35] CVX Research Inc. [Online]. Available: http://cvxr.com/cvx/

[36] G. Sharma and J. Martin, "MATLAB®: A language for parallel computing," *Int. J. Parallel Program.*, vol.37, no. 1, pp. 336, 2009.